

# Exploring the robustness of TractOracle methods in RL-based tractography

Jeremi Levesque<sup>a,\*</sup>, Antoine Théberge<sup>a</sup>, Maxime Descoteaux<sup>a</sup>, Pierre-Marc Jodoin<sup>a</sup>

<sup>a</sup>*Department of Computer Science, Faculty of Science, University of Sherbrooke, 2500  
Bd de l'Université, Sherbrooke, J1N 3C6, Québec, Canada*

---

## Abstract

Tractography algorithms leverage diffusion MRI to reconstruct the fibrous architecture of the brain's white matter. Among machine learning approaches, reinforcement learning (RL) has emerged as a promising framework for tractography, outperforming traditional methods in several key aspects. TractOracle-RL, a recent RL-based approach, reduces false positives by incorporating anatomical priors into the training process via a reward-based mechanism.

In this paper, we investigate four extensions of the original TractOracle-RL framework by integrating recent advances in RL, and we evaluate their performance across four diverse diffusion MRI datasets. Results demonstrate that combining an oracle with the RL framework consistently leads to robust and reliable tractography, regardless of the specific method or dataset used.

We also introduce a novel RL training scheme called *Iterative Reward Training (IRT)*, inspired by the Reinforcement Learning from Human Feedback (RLHF) paradigm. Instead of relying on human input, IRT leverages bundle filtering methods to iteratively refine the oracle's guidance throughout training. Experimental results show that RL methods trained with oracle feedback significantly outperform widely used tractography techniques in terms of accuracy and anatomical validity.

**Keywords:** Tractography, Diffusion MRI, Reinforcement learning

---



---

\*Code is available at <https://github.com/scil-vital/tractoracle-irt>

\*Corresponding author

Email address: [jeremi.levesque@usherbrooke.ca](mailto:jeremi.levesque@usherbrooke.ca) (Jeremi Levesque)

## 1. Introduction

Tractography is the computational process of reconstructing fibrous tissues using diffusion magnetic resonance imaging (dMRI) [1]. It is primarily employed to model white matter (WM) tracts in the human brain and remains the only non-invasive and reliable method for doing so. Accurate reconstruction of major neural pathways has proven valuable for various applications, including neurosurgical planning [2, 3], tractometry [4], and connectomics [5, 6].

Most traditional tractography algorithms operate by iteratively propagating streamlines following local diffusion information at or near the current tracking point. These methods determine the next tracking direction either deterministically—by following the maxima of a local diffusion model—or probabilistically—by sampling from the model interpreted as an orientation probability distribution [7].

A whole-brain tractogram that faithfully reflects anatomical reality is critical for downstream applications. However, despite algorithmic improvements, all traditional methods tend to generate a substantial proportion of anatomically invalid streamlines, known as false positives [8]. This stems from the inherent difficulty of the problem: attempting to reconstruct the brain’s global WM structure using only local diffusion information is fundamentally ill-posed [8]. In complex regions, such as fiber crossings or fanning areas [9], local cues are often insufficient to guide the tracking in a way that ensures both local coherence and global anatomical plausibility.

To tackle this issue, global tractography algorithms have been proposed [10]. These methods tend to minimize a cost function based on the alignment of streamline segments in each voxels [11, 12]. While appealing in theory, these methods tend to suffer from prohibitive computational costs. Moreover, the difficulty of imposing anatomical priors means that even in a *in silico* context without noise, these methods may not surpass traditional tractography [8].

Given that maintaining local coherence and global anatomical plausibility is a challenging task in tractography, post-processing techniques have been developed to filter out false positive streamlines. Examples include SIFT [13, 14], COMMIT [15], extractor\_flow [16], Verifyber [17] and FINTA [18]. A common strategy is to over-seed the brain—generating a surplus of streamlines—in the hope that, after filtering, most regions will retain enough anatomically plausible connections. However, this approach has notable drawbacks. First, filtering methods themselves are not infallible and

may be prone on filtering out rare, but valid, tracts, and second, over-seeding can significantly increase computational demands and runtime. Furthermore, in regions that are inherently difficult to track and yield a low proportion of true positives, filtering alone cannot recover missing streamlines and improve anatomical accuracy.

Supervised ML approaches have shown promise in addressing some limitations of traditional tractography methods [19, 20, 21, 22, 23]. These techniques require models to be trained on annotated streamlines, which involves manual validation by domain experts such as neuroanatomists and radiologists. However, this process is highly impractical for large-scale datasets due to the significant time and expertise required. Even assuming unlimited resources, the inherent variability between expert annotations makes it difficult to establish a reliable ground truth [24]. As a result, most datasets suitable for supervised learning in tractography, which are based on ground truths, are limited to *in silico* phantoms such as the FiberCup [25] and the ISMRM-2015 dataset [8], which may not fully reflect the complexity of human anatomy. Some *in vivo* datasets (e.g. TractoInferno [26], HCP105 [23]) were built to provide a standard structure and also provide a reference that can be used to train machine learning algorithms. In the case of TractoInferno, the reference streamlines were obtained using silver standard tractography algorithms as well as silver standard filtering algorithms which all have their own biases towards an accurate reconstruction of the anatomy. HCP105 has been semi-automatically annotated (as it involved some manual quality control and cleanup), but still suffer from incomplete regions (i.e. partially or fully missing bundles) due to using silver standard tractography algorithms. The inherent limitations of the reference streamlines essentially form a performance ceiling (w.r.t the anatomy) for downstream ML algorithms trained on such datasets.

Reinforcement learning (RL) has emerged as a viable alternative to supervised methods for tractography [27, 28, 29]. Unlike supervised learning, RL does not require reference streamlines which circumvents the limitations of the reference tracts from the *in vivo* datasets described above. Instead, a reward function guides the learning process of a so-called tractography agent. Early RL-based approaches used reward functions to mimic traditional algorithms—for instance, by rewarding alignment with the local dMRI signal orientation [27]. However, this formulation inherits the same limitations of local-only methods i.e., the inability to capture global anatomical context.

Moreover, stepwise reward structures are prone to reward hacking [30].

Since the agent receives rewards at each tracking step, it may learn to generate unnecessarily long streamlines that continue following plausible local directions—maximizing cumulative reward without ensuring anatomical validity. This behaviour frequently led to a significant number of false positives, despite the agent successfully optimizing its training objective.

To overcome these limitations, Théberge et al. [29] introduced *TractOracle*, a novel framework that integrates global anatomical knowledge into the RL training process using a so-called *oracle* neural network. This oracle is a transformer-based model trained on a silver standard set of streamlines, and is designed to evaluate the anatomical plausibility of candidate streamlines.

Once trained, the oracle is embedded into the RL framework in two key ways. First, it contributes to the reward function by providing a positive reward whenever the agent generates anatomically valid streamlines, encouraging more meaningful exploration during training. Second, during inference, the oracle acts as a stopping criterion—monitoring each in-progress streamline and terminating tracking if the growing path becomes implausible. This dual role allows the oracle to serve as both a guide and a gatekeeper, helping reduce the prevalence of anatomically invalid streamlines.

Empirical results demonstrated that this strategy substantially lowers the false positive rate, validating the effectiveness of incorporating non-local anatomical priors into the RL training pipeline.

This paper expands upon and reinforces the preliminary findings presented in TractOracle [29], offering a deeper analysis and broader empirical validation. We show that the core framework—integrating anatomical knowledge into the training process via a neural network oracle—is highly robust regardless of the RL-based tractography settings or any specific implementation choices. Whether updating the RL algorithm to a more modern variant, altering the number of streamline points passed to the oracle, enriching the agent’s input with broader local context or jointly training the oracle and the agent, the framework consistently outperforms state-of-the-art baselines in all scenarios. Additionally, with minor refinements to the agent’s training procedure, we further improve tracking accuracy, solidifying the framework’s lead over comparable methods.

The main contributions of this paper are the followings:

- We thoroughly validate the TractOracle framework with a variety of RL algorithms;
- We tackle the challenges of local tractography by endowing agents with a broader context window;
- We propose a new training scheme called *Iterative Reward Training* for RL-based tractography, improving the anatomical validity of reconstructed tractograms in vivo.

## 2. RL framework for tractography

### 2.1. Tractography

Tractography is the process of reconstructing WM pathways from dMRI. In this work we explore *iterative* tractography, where pathways (henceforth called *streamlines*, or *tracts*), represented by an ordered set  $P = \{p_0 \dots p_T\}$  where  $p_t \in \mathbb{R}^3$ , are obtained iteratively. From an initial 3D point  $p_0$ , the diffusion model (here a fiber ODF (fODF) [31, 32]), a vector field  $v$  is evaluated and a direction  $\mathbf{a}_0 \sim v(p_0)$  of amplitude  $\Delta$  is selected. The process iterates as  $p_{t+1} = p_t + \Delta \mathbf{a}_t$  until a stopping criterion is met, such as reaching the maximum streamline length, encountering a sharp angle between  $\mathbf{a}_{T-1}$  and  $\mathbf{a}_T$ , or stepping outside the white matter.

### 2.2. Reinforcement learning

RL models are commonly formalized as Markov Decision Processes (MDPs), where an agent  $\pi$  interacts with its environment through a set of states  $S$ , actions  $A$ , transition probabilities  $p(\mathbf{s}_{t+1}|\mathbf{s}_t, \mathbf{a}_t)$ , and rewards  $r(\mathbf{s}_t, \mathbf{a}_t)$ , abbreviated as  $r_t$ . The reward  $r_t$  can be seen as a return value that is high when the action  $a_t$  taken at state  $s_t$  is good and low when it is not.

In the context of tractography, the environment corresponds to the 3D diffusion signal—specifically, fODFs. The agent  $\pi_\theta$  is modelled as a neural network parameterized by  $\theta$ , which takes as input the state  $\mathbf{s}_t$ , a vector encoding the local environment around the current position  $p_t$ , and predicts an action  $\mathbf{a}_t$ , representing a direction of motion. The predicted action  $\mathbf{a}_t \sim \pi_\theta(\mathbf{s}_t)$  leads to a new state  $\mathbf{s}_{t+1}$  and a reward  $r_t$ .

By iteratively applying this process, a trajectory is formed, and the objective becomes to optimize the policy  $\pi_\theta$  to maximize the expected discounted return:

$$G_t = \sum_{k=t}^T \gamma^k r(\mathbf{s}_{t+k}, \mathbf{a}_{t+k}), \quad (1)$$

where  $\gamma \in [0, 1]$  is the discount factor, which favors immediate rewards when  $\gamma \rightarrow 0$ . The value function  $V_{\pi_\theta}(\mathbf{s}_t)$  estimates the expected return from state  $\mathbf{s}_t$ , while the action-value function (Q-function)  $Q_{\pi_\theta}(\mathbf{s}_t, \mathbf{a}_t)$  estimates the expected return of taking action  $\mathbf{a}_t$  in state  $\mathbf{s}_t$  before following policy  $\pi_\theta$ :

$$V_{\pi_\theta}(\mathbf{s}_t) = \mathbb{E}_{\pi_\theta}[G_t \mid \mathbf{s}_t], \quad (2)$$

$$Q_{\pi_\theta}(\mathbf{s}_t, \mathbf{a}_t) = \mathbb{E}_{\pi_\theta}[r_t + G_{t+1} \mid \mathbf{s}_t, \mathbf{a}_t]. \quad (3)$$

Optimizing  $\pi_\theta$  constitutes the core of RL research, with a wide range of algorithms proposed in the literature. One particularly effective algorithm for tractography applications is Soft Actor-Critic (SAC) [33], which was shown to be well suited for this domain [28]. SAC augments the standard RL objective by incorporating the policy’s entropy, promoting exploration and avoiding premature convergence:

$$G_t = \sum_{k=t}^T \gamma^k [r(\mathbf{s}_{t+k}, \mathbf{a}_{t+k}) + \alpha \mathcal{H}(\pi_\theta(\cdot \mid \mathbf{s}_{t+k}))], \quad (4)$$

where  $\alpha$  is a learned temperature parameter controlling the entropy term’s influence. The agent collects transitions in a replay buffer  $B$  and uses it to train both its Q-functions (parametrized by two neural networks, namely  $\phi_1$  and  $\phi_2$ ) and its policy  $\pi_{\theta}$  (also a neural network parametrized by  $\theta$ ) at each step. The target networks  $\phi'_1$  and  $\phi'_2$  are used to compute the Bellman residual.

See Appendix A.1 for a detailed explanation of Soft Actor-Critic. The reward will be described in the next subsections.

### 2.3. TractOracle

Theberge et al. [29] introduced a reward function with two components: a local term promoting the alignment between  $a_t$ , the fODF maxima  $v(p_t)$  at  $p_t$

and  $a_{t-1}$ , and an anatomical score of the reconstructed streamline. Formally:

$$r_t = \underbrace{\left( \left| \max_{\overline{v(p_t)}} \langle \overline{v(p_t)}, a_t \rangle \right| \cdot \langle a_t, a_{t-1} \rangle \right)}_{local} + \alpha \underbrace{\mathbb{1}_{\Omega_\psi}(P_{0..t})}_{anatomical} \quad (5)$$

$$\mathbb{1}_{\Omega_\psi}(P_{0..t}) = \begin{cases} 1 & \text{if } \Omega_\psi(P_{0..t}) \geq 0.5 \text{ and } t = T \\ 0 & \text{else,} \end{cases} \quad (6)$$

with  $\Omega_\psi$  *TractOracle-Net*, a transformer-based neural network [34] trained to assess the anatomical validity of streamlines. In other words, when a P-long streamline  $P_{0..t}$  is deemed anatomically plausible, i.e. when TractOracle-Net  $\Omega_\psi(P_{0..t}) \geq 0.5$ , the reward at step  $t$  is augmented by a factor  $\alpha$ .

TractOracle-Net, which we will refer to as *an oracle*, is a transformer with 4 transformer encoding blocks each having 4 multi-attention heads, totalling 550K parameters. For a detailed architecture illustration, please refer to Appendix B.

### 3. Methodology

In order to demonstrate how effective the use of an oracle is in RL-based tractography, we introduce several improvements to *TractOracle* to align it with recent best practices in RL. Specifically, we generalize the framework to support a broader range of RL algorithms, enhance the state representation, and implemented a strategy to better align the reward function with the learned policies. These methods are described in the following four subsections. The reader may also find further technical details in the supplementary material from Appendix A to Appendix C.

#### 3.1. Oracle

In this work, we expand upon the experimental procedure of [29] by training oracles and agents on mutiple datasets and using multiple filtering methods as reference. Namely, on the in silico dataset (c.f. section 4.1), we use local and PFT [35] tracking to generate reference streamlines which are then resampled to a fixed number of points and then annotated by the Tractometer [36] as true or false positives. On the in vivo HCP dataset (c.f. 4.1), we again use local and PFT [35] tracking but instead use Verifyber, extractor\_flow and RecobundlesX to provide three annotations per streamline,

which are then used to train three oracles. Finally, on the in vivo TractoInferno dataset, we repeat the tracking procedure of [29] and annotate the streamlines using the previous three methods. In all cases, to train the oracles, we split the annotated reference streamlines in training (80%), validation (10%) and testing (10%) sets. In addition to filtering methods, we also explore how varying the number of points used to resample streamlines affects the prediction accuracy. Indeed, Théberge et al [29] trained their oracle using streamlines resampled to 128 points. However, previous work has shown that streamlines can be effectively compressed to far fewer points—as few as 12—without significant loss of information [37, 38]. Given that transformer models relying on self-attention scale quadratically with sequence length [34], and that TractOracle-Net is invoked at every tracking step, using shorter sequences is computationally advantageous. In this work, we therefore consider oracles trained with streamlines resampled to 32 points. We additionally explore the impact of the number of points per streamlines in section 4.2. Oracles were trained using a mean squared error loss. For an brief list of the hyperparameters used, refer to table E.5.

### 3.2. *DroQ*

While SAC has been the defacto model-free RL algorithm since its proposal, several papers [39, 40, 41] have outlined its sample inefficiency: many transitions need to be sampled from the environment to properly train agents. Numerous improvements over SAC have been proposed over the years. One such method is Dropout Q-Functions (DroQ) [41], a reinforcement learning algorithm that builds on SAC. Essentially, DroQ performs training updates more frequently while collecting fewer transitions which improves SAC’s sample efficiency. As naively increasing the number of updates can destabilize learning, the authors introduce additional tricks to address this issue. Additional details on the modifications done are detailed in Appendix A.2. Experimental results demonstrate that these modifications lead to higher returns with fewer environment interactions compared to SAC and other related methods.

### 3.3. *CrossQ*

CrossQ [42] is another approach aimed at improving the SAC algorithm. Developed concurrently with DroQ, CrossQ seeks to simplify SAC while enhancing its sample efficiency. To achieve this, the authors remove the target



critic networks and carefully incorporate Batch Normalization (BatchNorm) layers [42] into the Q-networks.

A key detail in their approach is the treatment of state-action pairs: tuples  $(s_k, a_k)$  and  $(s_{k+1}, a_{k+1})$  are concatenated *batch-wise* to ensure they are processed as part of the same distribution. This design allows both to contribute equally to BatchNorm’s running statistics, which helps stabilize training. The authors argue that these simplifications not only simplify the architecture but also lead to improved performance and sample efficiency.

For more details on CrossQ, please refer to Appendix A.3.

### 3.4. Widening neighbourhood signal

Previous work on the formulation of the state  $\mathbf{s}_t$  in RL-based tractography [28, 43] has primarily focused on *local* representations—typically limited to a small neighborhood of voxels surrounding the current position  $p_t$ . However, relying solely on local information exacerbates the inherently ill-posed nature of tractography. To mitigate this limitation, we explore expanding the spatial context provided to the agent by increasing the radius of voxels included in the input.

Earlier methods, including *TractOracle* [29], use only the six immediate neighbors of  $p_t$ —corresponding to the adjacent voxels in the up, down, left, right, anterior, and posterior directions (see figure1)(a)). Given that each voxel encodes 28 spherical harmonics coefficients, this results in a feature vector of size  $28 \times 7 = 196$ .

In this work, we incorporate a larger 4D window of size  $N \times N \times N \times 28$  centered at  $p_t$ . As illustrated in figure 1 (b), this voxel cube is processed by an convolutional encoder that outputs a 4D tensor of shape  $3 \times 3 \times 3 \times 32$ , where 32 denotes the number of output channels. This tensor is then flattened into a 1D vector of length 864, which is used as input to the agent. The sheer reason for using an encoder is to reduce the size of the input data as we empirically found that a raw  $N \times N \times N \times 28$  bloc leads to poor results when  $N > 5$ .

Consistent with the *TractOracle* architecture, both state formulations concatenate this vector with the previous 100 tracking directions to form the final state  $\mathbf{s}_t$ .

### 3.5. Iterative reward training (IRT)

It is well known that different tracking algorithms produce different looking streamlines, and consequently streamlines from different algorithms may

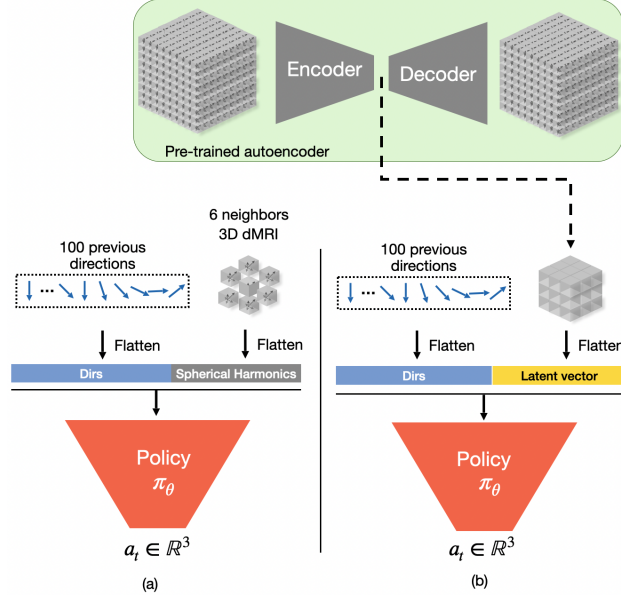


Figure 1: Different state formulations. (a) State formulation as presented in [27] using the spherical harmonics to the 6 closest neighbours of  $p_t$ . (b) An encoder encodes a volume of  $N \times N \times N$  voxels each having 28 diffusion MRI spherical harmonics coefficients into a  $3 \times 3 \times 3 \times 32$  tensor that is flattened and given to the agent as a vector of length 864. In both cases, the 100 last tracking steps are included [28]. Details about the training of the autoencoder as well the encoder and decoder architectures are provided in Appendix C

have a different *shape distribution*. Empirically, we found that streamlines produced by RL-based algorithms follow this trend, including TractOracle-RL.

We therefore hypothesize that TractOracle-Net, the streamline evaluation network introduced in TractOracle [29] trained solely on streamlines tracked by classical methods, may suffer from *distributional shift* when scoring streamlines produced by TractOracle-RL.

In order to tackle this distribution shift, we propose to iteratively train the oracle jointly with the RL agent, inspired by Reinforcement Learning from Human Feedback (RLHF) methods (like ChatGPT) [44]. We name this process *iterative reward training* (IRT) and refer the reader to figure 2 for a step-by-step illustration of IRT and to figure 3 for a comparison with other RL-based tractography methods. This procedure aims to *align* the distribution of streamlines produced by RL-tracking methods with the distribution of streamlines used to trained the oracle. We aim to keep the performance

of the oracle so that it is on-par or better with what was measured during its initial training process.

IRT is a three-step method. First, the RL agent  $\pi_\theta$  is trained with the initial oracle until it reaches a plateau (about 150-200 episodes). Then, the agent generates tractograms for a subset of randomly-picked subjects (here 5 subjects) from the training dataset until approximately 250K streamlines are accumulated using the current policy. The tractograms are then filtered by RecobundlesX [45], extractor\_flow [16] or Verifyber [17] so their streamlines are annotated as plausible or implausible, similar to the workflow described in section 3.1. The annotated tracts are then split into training, validation and testing sets each holding 80%, 10%, 10% of the examples before being appended to the dataset which includes annotated tracts from previous iterations.. Finally, the oracle is trained for a few epochs. Then, the RL training loop goes back to step 1 where the tracking agent is trained some more. The process is repeated until the agent has performed 3000 episodes of training.

On the first IRT iteration, we train the oracle for 5 epochs so it can quickly recover a good prediction accuracy on tractograms generated by RL-based tractography algorithms. On subsequent IRT iterations, we train the oracle for a single epoch as we train the oracle relatively often compared to the rate of behaviour change of the RL agent. In other words, the shape distribution of the streamlines should change only slightly in between each IRT iteration and we hypothesize that training for a single epoch is done to essentially maintain the good prediction accuracy during the whole RL agent training.

We limit the size of the dataset to 4M streamlines, leading to the "earlier" streamlines being overwritten after a few iterations. As the training improves the performance of the agent, the agent should be more and more biased towards reconstructing plausible (i.e. valid) streamlines. With this in mind, before appending new data to the dataset, we randomly sample the over represented class to match the number of streamlines of the under represented class, which keeps the dataset balanced with 50% plausible and 50% implausible streamlines. The data was carefully split in training, validation and testing sets in order to keep each separate dataset balanced so that we're never in a scenario with any class that is over-represented.

### 3.6. Tracking agents

The policy  $\pi_\theta$  as well as the Q-networks and the value functions are all four-layer multilayer perceptrons with three hidden linear layers of size 1024

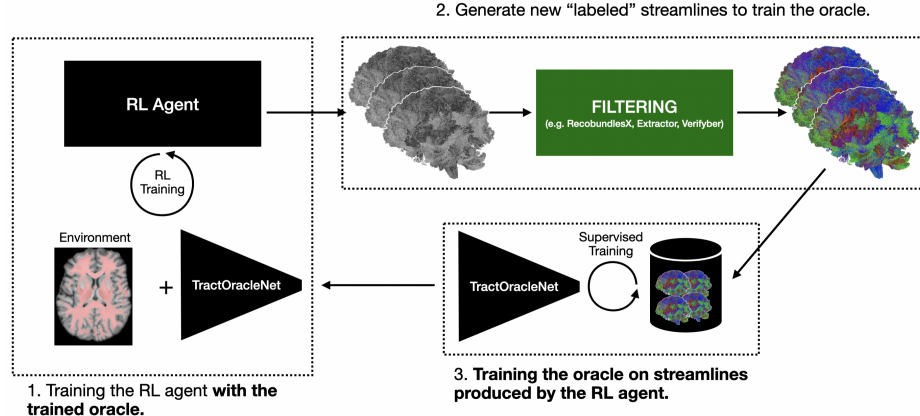


Figure 2: The 3-step Iterative Reward Training (IRT) method. **Step 1.** The RL agent is trained for a limited number of epochs. **Step 2.** The agent generates whole-brain tractograms for a set of training subjects randomly selected from the dataset. The resulting streamlines are classified as being anatomically plausible or implausible using a filtering method. The streamlines generated at each iteration are accumulated in a growing dataset. **Step 3.** The oracle is fine-tuned for a few epochs using the updated dataset, after which the process returns to Step 1.

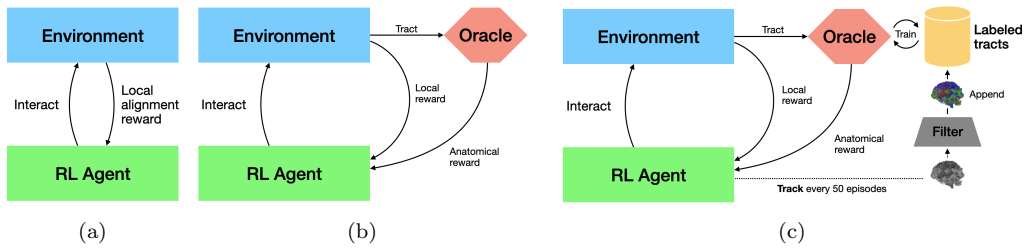


Figure 3: Evolution of RL-based tractography training paradigms. **(a)** Track-to-Learn (TTL): the agent trains by optimizing the local alignment reward at each tracking step. **(b)** TractOracle: the agent is train to jointly optimize the local reward and the additional anatomically-informed reward. **(c)** Iterative reward tuning: the reward model is iteratively aligned with the filtering method.

and a final output layer of size 3 or 1 for the policy and the critic respectively.

To assess the impact of extended training, we also evaluated a variant trained for 3,000 episodes, denoted *SAC-3K*, to observe whether prolonged training could potentially cause divergence or reward hacking problems. Additional variants include *DroQ-1K* and *CrossQ-3K*, which respectively incorporate the DroQ and CrossQ RL algorithms. *CrossQ-3K* is trained for 3,000 episodes while we trained DroQ-1K for 1,000 episodes due to its slower run time and higher sample efficiency. We also introduce *CrossQ-AE*, a CrossQ-based variant that leverages the latent space encoding described in Figure 1(b).

Finally, we implement two versions of TractOracle trained with the iterative reward training (IRT) scheme: *SAC-IRT* and *CrossQ-IRT*.

In order to quantify and effectively evaluate each tracking experiment, we use different strategies to assess the performance of the different methods. Upon training and tracking on in silico datasets, we utilize the Tractometer [36] to provide 8 different metrics (which are listed and detailed in Appendix D) that we use to compare the different algorithms. However, since the in vivo datasets do not provide ground truth tract annotations, we leverage RecobundlesX [45, 38], extractor\_flow [16] and Verifyber [17] to quantify the number of streamlines recognized by each method.

Since *in vivo* datasets do not provide ground truth streamlines or tract annotations, for all methods

## 4. Experiments and results

### 4.1. Datasets

Five datasets were used in the following experiments.

- 1) **ISMIRM2015** is synthetic dataset generated from a single subject from the Human Connectome Project [8, 46]. Global tractography was performed on the subject and 25 reference bundles were manually segmented. FiberFox [47] was used to generate a synthetic diffusion volume (2mm iso, 32 directions, b=1000) and T1w image from the segmented bundles. We repeat the experimental procedure of Theberge et al. [29] and tracked  $\sim 1$ M streamlines with five classical tractography algorithms [48, 35, 49] using each’s default set of parameters, seeding in both the WM and the WM-GM interface. Streamlines were then input to the Tractometer [36] to obtain true positives and false positives, acting as labelled data to train the oracles.

- 2) **BIL & GIN** [50] is a publicly-available dataset of 453 healthy adults mostly in their twenties. All acquisitions were performed on a Philips Achieva 3T scanner using 21 non-colinear diffusion gradient directions, a b-value of 1,000 s/mm<sup>2</sup>, four signal averages, and an isotropic resolution of 2 mm. Following the experimental setup by Legaretta et al. [18], we focus on the callosal streamlines of 39 subjects; specifically on homotopic streamline bundles—those connecting gyral-based segment pairs across hemispheres—within 26 predefined anatomical regions, which are treated as plausible anatomical connections for training TractOracle-Net, while everything else is treated as unplausible. For more details on these bundles and how they were extracted, please refer to section A5 of Legaretta et al. [18].
- 3) **TractoInferno** [26] is a publicly accessible and highly diverse dataset developed to support machine learning applications in diffusion MRI (dMRI) tractography. It includes data from 354 individuals, aggregated from six distinct sources and acquired using five different MRI scanners, encompassing a wide range of resolutions, acquisition protocols, and participant age groups. All MRI scans underwent manual quality control prior to tractography, which was performed using an ensemble of four methods: local deterministic, local probabilistic, PFT [35], and SET [49]. The resulting streamlines were then processed using RecoBundlesX to produce a silver-standard reference.
- 4) **Human Connectome Project (HCP)** is a collection of *in vivo* subjects, of which we randomly selected 100. Each subject’s diffusion image was acquired at 1.25mm iso using 288 directions over three shells (b=1000, 2000, 3000) [51]. Each subject was processed using TractoFlow [52] to obtain fODFs, peaks, tissue segmentations and T1w images registered in the diffusion space. We use 80 subjects for training, 10 for validation and 10 for testing.
- 5) **Penthera 3T** [53] is a dataset of 12 healthy individuals of an average age of  $25.92 \pm 1.86$ . Each subject was scanned 6 times: 3 times per session for 2 sessions. Each diffusion image was acquired at 2.0mm iso over three shells (b=300, 1000, 2000) on 8, 32, and 60 distributed directions respectively. Each subject was using TractoFlow [52] to obtain fODFs, peaks, tissue segmentations and T1w images registered in the diffusion space at a resolution of 1mm iso. From this dataset, we use the first two scans of the first session for the 12 subjects for a total of 24 acquisitions.

For all datasets, we use fODFs of order 6 (28 spherical harmonics coefficients) as fODFs of order 8 were too computationally expensive and order 4 were too low frequency. FODFs of order 6 ended up being a good compromise between a good representation and computational efficiency. Furthermore, we used 6 to replicate the experimental setup of previous RL tractography method that we compare our methods to [27, 29].

#### 4.2. Experiment 1: number of points

For the first experiment, we explore the impact of the number of points per streamline used to train oracles. We consider streamlines resampled to 32, 64 and 128 points on the ISMRM2015 and BIL&GIN datasets.

#### 4.3. Experiment 2: *in silico* tracking

In this experiment, we evaluate the performance of our RL tracking agents, SAC, DroQ, CrossQ and their variants on the ISMRM2015 dataset using the metrics extracted by the Tractometer. We perform an experiment on a synthetic dataset first to essentially conclude whether our methods and their variants are effective candidates for *in vivo* tracking. It is easier to quickly compare and analyze the generation performance of different algorithms using a well-defined ground truth that provides extensive metrics.

We compare our methods against three well-known non-ML tractography algorithms, namely **sd\_stream** and **iFOD2** from MRTrix3 [48] and Parallel Transport Tractography [54] (**PTT**) from Trekker as well as two reinforcement learning-based approaches: the original **Track-to-Learn** (TTL) method [27] and the more recent **TractOracle** framework [29], referred to as SAC-1k from now on.

#### 4.4. Experiment 3: *in vivo* tracking

In this experiment, we compare the same tracking methods as the previous experiment, but on *in vivo* images where we can truly assess the generation capabilities of our algorithms on real-world data. The objective of this experiment is to evaluate which methods yield a higher number of true positive streamlines. All machine learning-based tracking methods were trained and tested on both the TractoInferno and HCP datasets using 20 seeds per voxel. From this point onwards, we omit DroQ and CrossQ-AE as their training is significantly slower and the tracking speed of CrossQ-AE is prohibitively slow as we highlight in section 4.6.2 below.

Table 1: Classification metrics on the ISMRM2015 and BIL&GIN datasets. RecobundlesX and FINTA results are reported from [55].

ISMRM2015					
	Accuracy	Sensitivity	Precision	F1-score	Time(s)
RecobundlesX	0.91	0.81	0.97	0.88	-
FINTA	0.91	0.91	0.91	0.91	-
TractOracle-Net-128	<b>0.98</b>	0.98	0.97	<b>0.98</b>	21
TractOracle-Net-64	<b>0.98</b>	<b>0.99</b>	0.97	<b>0.98</b>	10
TractOracle-Net-32	<b>0.98</b>	0.98	<b>0.98</b>	<b>0.98</b>	<b>6</b>
BIL&GIN					
	Accuracy	Sensitivity	Precision	F1-score	Time(s)
RecobundlesX	0.82	0.80	0.67	0.70	-
FINTA	0.91	<b>0.91</b>	<b>0.78</b>	<b>0.83</b>	-
TractOracle-Net-128	0.95	<b>0.91</b>	0.74	0.82	20
TractOracle-Net-64	0.95	<b>0.91</b>	0.75	0.82	10
TractOracle-Net-32	<b>0.96</b>	<b>0.91</b>	0.76	<b>0.83</b>	<b>6</b>

#### 4.5. Experiment 4: transfer learning

In this experiment, we assess the generalization capability of our agents by testing them on entirely different datasets without performing any additional fine-tuning. To ensure consistency with the prior evaluations, we generate the tractograms using the same procedure as in the previous section—specifically, using 20 seeds per voxel.

All experiments are run using a single GPU, either a NVidia RTX4090 or a NVidia V100SXM2, as the training of most models does not require more than 4Gb of VRAM, with the exception of training the oracle where 32Gb of VRAM is recommended. Although training our experiments require the use of GPUs, utilizing the trained models afterwards is much less memory-consuming and can easily be performed on a consumer laptop.

#### 4.6. Results

##### 4.6.1. Scoring streamlines resampled to fewer number of points

Results on the ISMRM2015 and BIL&GIN datasets are presented in Table 1. Reducing the number of points per streamline does not degrade oracle classification performance, but significantly reduces inference time. Based on these findings—and since no performance drop was observed when using TractOracle-Net-32 instead of TractOracle-Net-128 during TractOracle-RL training—we adopted the 32-point streamlines.



Table 2: Tractometer scores on ISMRM2015. Scores in **bold** indicate the best method for each metric, in **blue** are methods that severely underperformed and underlined is the best method with an oracle at their core. 1K and 3K stand for the number of training episodes. For conciseness, all methods below the double horizontal line (i.e. SAC, CrossQ, DroQ) refer to a TractOracle experiment. Appendix D offers a detailed list of the acronyms used to identify the metrics in this table.

	VC % $\uparrow$	VB (/21) $\uparrow$	IC % $\downarrow$	IB $\downarrow$
sd_stream	55.96 $\pm$ 0.21	19.00 $\pm$ 0.00	<b>44.04 <math>\pm</math> 0.21</b>	199.80 $\pm$ 4.26
ifod2	<b>31.53 <math>\pm</math> 0.20</b>	19.00 $\pm$ 0.00	<b>68.47 <math>\pm</math> 0.20</b>	<b>281.00 <math>\pm</math> 4.00</b>
ptt	<b>26.41 <math>\pm</math> 0.05</b>	19.40 $\pm$ 0.55	<b>54.44 <math>\pm</math> 0.03</b>	<b>457.40 <math>\pm</math> 4.62</b>
TTL [27]	66.13 $\pm$ 1.15	<b>20.00 <math>\pm</math> 0.63</b>	<b>33.87 <math>\pm</math> 1.15</b>	<b>293.40 <math>\pm</math> 11.8</b>
SAC-1K [29]	88.05 $\pm$ 0.35	19.00 $\pm$ 0.47	11.95 $\pm$ 0.35	195.67 $\pm$ 4.99
SAC-3K	90.73 $\pm$ 0.05	19.00 $\pm$ 0.00	9.08 $\pm$ 0.05	151.20 $\pm$ 2.05
DroQ-1K	84.80 $\pm$ 0.05	19.00 $\pm$ 0.00	14.86 $\pm$ 0.05	171.20 $\pm$ 3.27
CrossQ-3K	<b>91.64 <math>\pm</math> 0.04</b>	19.00 $\pm$ 0.00	<b>8.11 <math>\pm</math> 0.03</b>	159.40 $\pm$ 4.51
CrossQ-AE	85.88 $\pm$ 0.03	17.00 $\pm$ 0.00	13.66 $\pm$ 0.04	<b>142.00 <math>\pm</math> 4.06</b>
SAC-IRT	89.17 $\pm$ 0.03	19.00 $\pm$ 0.00	10.58 $\pm$ 0.03	173.60 $\pm$ 3.13
CrossQ-IRT	84.45 $\pm$ 0.06	<u>19.33 <math>\pm</math> 0.00</u>	15.00 $\pm$ 0.07	172.40 $\pm$ 7.99
	OL % $\uparrow$	OR $\downarrow$	F1 % $\uparrow$	NC $\downarrow$
sd_stream	38.85 $\pm$ 0.05	<b>3.59 <math>\pm</math> 0.05</b>	52.47 $\pm$ 0.03	<b>9.36 <math>\pm</math> 0.18</b>
ifod2	48.70 $\pm$ 0.11	8.18 $\pm$ 0.19	59.10 $\pm$ 0.07	<b>12.45 <math>\pm</math> 0.08</b>
ptt	<b>75.32 <math>\pm</math> 0.14</b>	32.45 $\pm$ 1.43	<b>65.75 <math>\pm</math> 0.18</b>	<b>19.15 <math>\pm</math> 0.05</b>
TTL [27]	53.84 $\pm$ 2.28	29.94 $\pm$ 2.00	57.43 $\pm$ 1.84	2.85 $\pm$ 0.42
SAC-1K [29]	<u>48.43 <math>\pm</math> 0.64</u>	17.68 $\pm$ 1.00	<u>57.00 <math>\pm</math> 0.47</u>	0.73 $\pm$ 0.12
SAC-3K	35.43 $\pm$ 0.03	15.25 $\pm$ 0.29	45.87 $\pm$ 0.05	<b>0.19 <math>\pm</math> 0.01</b>
DroQ-1K	38.24 $\pm$ 0.05	21.10 $\pm$ 0.15	47.00 $\pm$ 0.07	0.34 $\pm$ 0.01
CrossQ-3K	33.20 $\pm$ 0.08	15.53 $\pm$ 0.11	43.27 $\pm$ 0.08	0.25 $\pm$ 0.01
CrossQ-AE	25.63 $\pm$ 0.05	23.61 $\pm$ 0.15	31.04 $\pm$ 0.09	0.46 $\pm$ 0.01
SAC-IRT	35.77 $\pm$ 0.12	<u>15.05 <math>\pm</math> 0.13</u>	45.85 $\pm$ 0.15	0.25 $\pm$ 0.01
CrossQ-IRT	33.90 $\pm$ 0.10	15.26 $\pm$ 0.25	44.22 $\pm$ 0.11	0.54 $\pm$ 0.01

#### 4.6.2. In silico results : ISMRM2015

The Track-to-Learn variants introduced in section 3.6 were first evaluated on the in silico dataset. Results are presented in Table 2 -please refer to the supplementary material for a detailed description of the eight evaluation metrics.

As shown in the table, methods that do not rely on an oracle (i.e., sd\_stream, ifod2, ptt and Track-to-Learn) achieve top performance on some metrics —namely, the number of valid bundles (VB), overlap (OL), overreach (OR), and F1-score—while performing poorly on others, such as valid and invalid connections (VC, IC), invalid bundles (IB), and the number of no connections (NC).

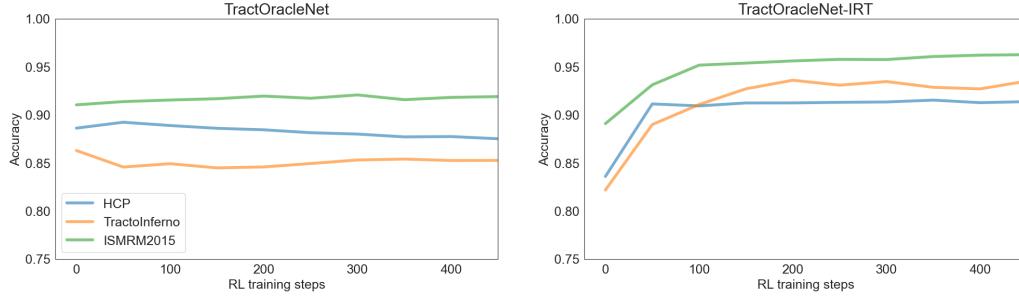


Figure 4: Accuracy of the reward network during the training steps without IRT (left) and with IRT (right) with RecobundlesX as a reference.

In contrast, the oracle-based methods exhibit more balanced performance across all metrics. They also achieve highly competitive results on key indicators, including the proportion of valid and invalid connections (VC + IC), the number of valid bundles (VB), the number of invalid bundles (IB), and, most notably, the percentage of no connections (NC).

Furthermore, it is important to highlight that the training of *DroQ* and *CrossQ-AE* is significantly slower—by a factor ranging from  $10\times$  to  $30\times$  compared to the other methods. Additionally, the tracking speed of *CrossQ-AE* is prohibitively slow. For these reasons, and given that neither method demonstrated superior performance, we decided not to include them in the subsequent experiments.

#### 4.6.3. In vivo results : HCP and TractoInferno

We report in Table 3 the number of streamlines deemed anatomically plausible by each filtering algorithm for each experiment. In each experiment, in order to emphasize which reference filtering method was used in the agents’ training, we highlight the corresponding column in gray. We quickly notice, that all proposed methods significantly outperform the four baseline methods, producing on average between  $3\times$  and  $20\times$  more valid streamlines than *sd\_stream*, *ifod2* and *ptt*, across both datasets. We also see how the use of an oracle drastically improves the performance of baseline RL methods such as *Track-to-Learn*, in almost all scenarios. Now, we notice that, as the length of the training extends, the agent specializes on tracking according to the inherent anatomical constraints posed by the different reference methods. A good example of this would be using the *extractor\_flow* as a reference for *TractoInferno* (i.e. *EXT-ref*) where the number of plau-

sible streamlines is high both for RecobundlesX and extractor\_flow when tracking using *SAC-3K*. However, as the performance keeps increasing for extractor\_flow when introducing the IRT scheme, the number of plausible streamlines for RecobundlesX crumbles to less than half the number from *SAC-3K*. Other similar scenarios in our experiments from table 3, but in most cases the number of plausible streamlines increase even when the filtering algorithm isn't used as a reference for the corresponding experiment. We notice that, specifically for the *RBX-ref* experiment on HCP, the number of plausible streamlines remains essentially the same across the different training regimes for the oracle-based RL agents, but still exceeds the other non-oracle methods by a factor of up to 4.

Figure 5 displays a few bundles from subject 1006 of the TractoInferno dataset which were tracked using baseline methods as well as the proposed methods which were trained on the same dataset. For the sake of conciseness, we selected a subset of the different methods which also reflects the performance of the other variants. With this figure, we showcase the qualitative improvements of our proposed methods compared to the baseline methods. Visually, our proposed methods produce more anatomically plausible and densely reconstructed bundles with clear fanning and improved spatial coherence. This is particularly evident for the IRT-based method, which, as reported in Tables 3 and 4, generally yields the highest number of true positive streamlines among all tested approaches. We also notice that some bundles (e.g. the uncinatus fasciculus) are more easily reconstructed by RL-based methods and more clearly structured when using the IRT training procedure.

#### 4.6.4. Transfer learning: *Penthera-3T*, *TractoInferno* and *HCP*

Table 4 presents the number of streamlines recovered by RecoBundlesX in a transfer learning setting. Agents trained on the HCP dataset were evaluated on the TractoInferno datasets, while agents trained on TractoInferno were tested on both the HCP and Penthera-3T datasets.

We observe that the agents trained on TractoInferno generalize very well on both the HCP and Penthera-3T datasets as all oracle-based methods produce an average between 2 to 7 times more plausible streamlines than baseline methods. Those generalization results are illustrated in figure 6. We notice that for *SAC-IRT*, especially for the parieto-occipito pontine tracts, the pyramidal tracts and the inferior longitudinal fasciculus, the bundles are much more dense and have wider fanning than other methods. For other

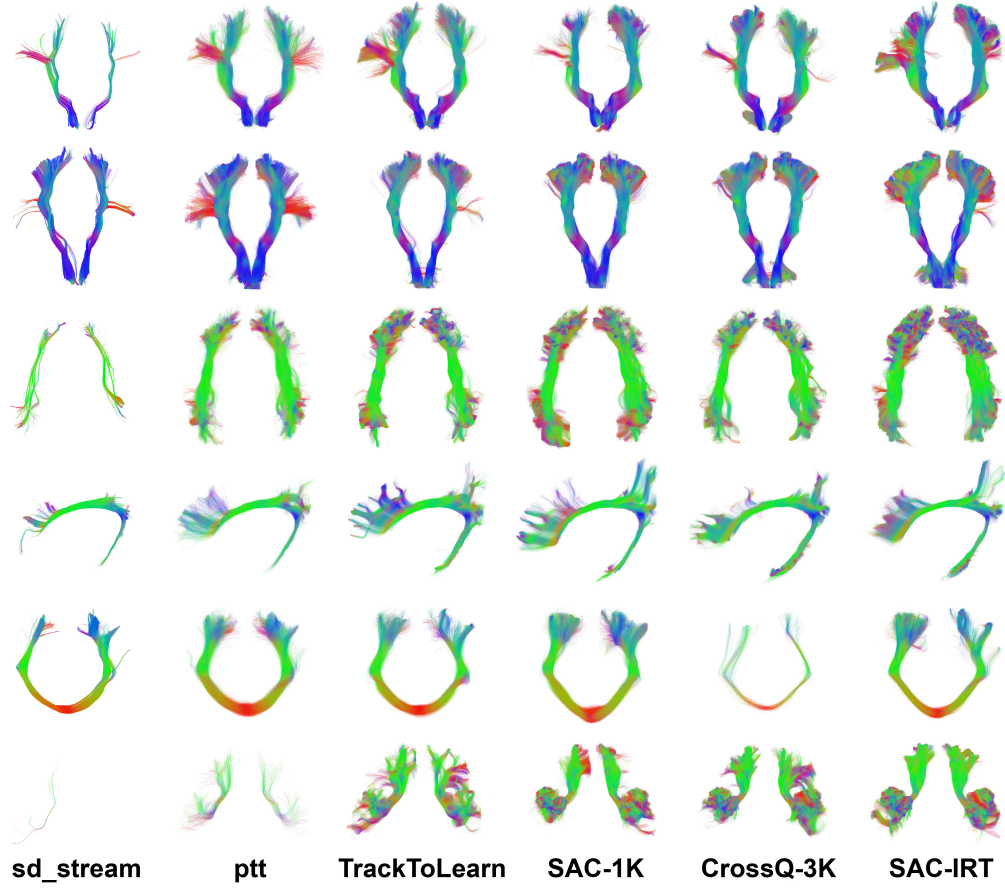


Figure 5: Visualization of the parieto-occipito pontine tract (1st row), pyramidal tract (2nd row), inferior longitudinal fasciculus (3rd row), left cingulum (4th row), occipital lobe of the corpus callosum (5th row), right and left uncinate fasciculus (last row) for the **subject 1006 of the TractoInferno dataset**. For all methods, results were produced by tracking with 5M seeds each (distributed uniformly across the seeding mask).

Table 3: Total number of streamlines recovered by RecobundlesX (RBX) [38], extractor\_flow (EXT) [16] and Verifyber (VER) [17] on the TractoInferno and HCP datasets for all tracking algorithms. Proposed RL agents were rewarded with different oracles across 3 experiments. Each experiment denoted by the headers RBX-ref, EXT-ref and VER-ref were conducted using the same procedures with the exception of the reference method used to score the streamlines during the oracles’ initial training was RecobundlesX, extractor\_flow and Verifyber respectively. The grayed columns highlights the reference method used to train the oracle for each experiment. The number of streamlines should be maximized and the best result is highlighted in **bold**.

	Method	RBX-ref			EXT-ref			VER-ref		
		RBX	EXT	VER	RBX	EXT	VER	RBX	EXT	VER
TractoInferno	sd_stream	1,6M	6,0M	56,6M	1,6M	6,0M	56,6M	1,6M	6,0M	56,6M
	ifod2	8,0M	9,7M	83,0M	8,0M	9,7M	83,0M	8,0M	9,7M	83,0M
	ptt	8,7M	16,0M	82,7M	8,7M	16,0M	82,7M	8,7M	16,0M	82,7M
	TTL	9,2M	12,4M	84,3M	9,2M	12,4M	84,3M	9,2M	12,4M	84,3M
	SAC-1K	20,8M	<b>21,0M</b>	103,7M	10,4M	22,2M	110,6M	8,0M	19,2M	117,6M
	SAC-3K	21,6M	12,8M	93,0M	<b>29,8M</b>	24,4M	110,2M	17,4M	19,4M	118,5M
	CrossQ-3K	21,4M	11,9M	81,3M	25,6M	23,5M	110,3M	<b>21,5M</b>	<b>21,6M</b>	122,6M
	SAC-IRT	<b>33,4M</b>	15,3M	<b>104,7M</b>	13,6M	24,9M	<b>116,7M</b>	16,9M	16,2M	120,4M
	CrossQ-IRT	31,7M	15,0M	95,8M	15,4M	<b>25,2M</b>	111,7M	16,7M	18,6M	<b>123,8M</b>
HCP	sd_stream	688K	880K	5,8M	687,5K	879,9K	5,8M	687,5K	880K	5,8M
	ifod2	769,7K	1,5M	12,0M	769,7K	1,5M	12,0M	769,7K	1,5M	12,0M
	ptt	2,1M	2,1M	11,4M	2,1M	2,1M	11,4M	2,1M	2,1M	11,4M
	TTL	2,2M	2,3M	11,4M	2,2M	2,3M	11,3M	2,2M	2,3M	11,3M
	SAC-1K	7,7M	2,8M	12,9M	1,9M	2,9M	13,9M	1,3M	2,3M	14,5M
	SAC-3K	7,0M	2,2M	<b>13,5M</b>	3,1M	3,6M	13,5M	4,3M	2,5M	15,4M
	CrossQ-3K	<b>8,4M</b>	<b>2,9M</b>	13,4M	3,3M	3,4M	14,3M	3,7M	2,9M	15,3M
	SAC-IRT	7,4M	2,7M	12,5M	4,5M	<b>4,0M</b>	14,2M	<b>7,5M</b>	2,9M	<b>16,4M</b>
	CrossQ-IRT	7,4M	2,6M	12,8M	<b>4,6M</b>	3,9M	<b>14,6M</b>	6,5M	<b>3,2M</b>	16,0M

illustrated bundles, SAC-IRT and other oracle-based algorithms are on-par or better than other non oracle-based algorithms in terms of bundle density, fanning and spatial coherence.

Although the generalization capabilities of the *SAC-IRT* and *CrossQ-IRT* algorithms trained on the HCP dataset do not stand out as much as in Table 4 compared to other oracle-based methods, they are on-par with them. Overall, all the oracle-based algorithms still outperform the other tractography methods.

## 5. Discussion

The results presented in this work highlight two key findings. First, incorporating an oracle into an RL-based tractography system consistently provides a significant advantage. Regardless of the underlying RL algorithm—whether SAC, DroQ, or CrossQ—or whether the system is trained with or without Iterative Reward Training (IRT) or extended spatial context, oracle-guided RL methods systematically outperform both oracle-free RL approaches (such as Track-to-Learn) and traditional tractography techniques

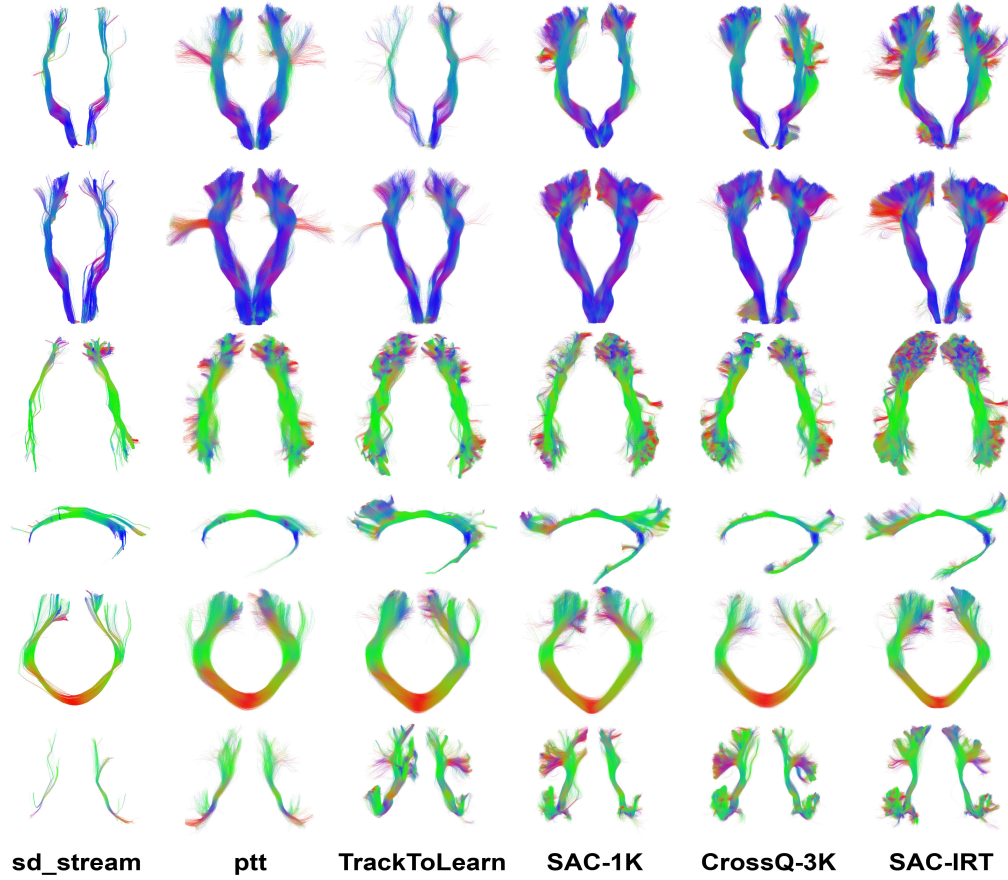


Figure 6: Visualization of the transfer learning experiment by **tracking on the Penthera-3T dataset after training on TractoInferno**. Visualizations are of the parieto-occipito pontine tract (1st row), pyramidal tract (2nd row), inferior longitudinal fasciculus (3rd row), left cingulum (4th row), occipital lobe of the corpus callosum (5th row), right and left uncinate fasciculus (last row) on the first scan of the first session of the subject 01 from the Penthera-3T dataset. For all methods, results were produced by tracking with 4,5M seeds each (distributed uniformly across the seeding mask).

Table 4: Total number of streamlines recovered by RecobundlesX [38] in a **transfer learning** setting for the TractoInferno, HCP, and Penthera-3T datasets using all previous agents. **HCP**  $\rightarrow$  **TractoInferno** indicate that the agent was trained on HCP and tested on TractoInferno. Similarly, for the entry **TractoInferno**  $\rightarrow$  **Penthera-3T**, the agent was trained on TractoInferno while the tracking was done on the Penthera-3T dataset and so on. Results from sd\_stream, ifod2 and ptt are reported from table 3. Results in **bold** outperform others.

	<b>HCP</b> ↓	<b>TractoInferno</b> ↓	<b>TractoInferno</b> ↓
<b>Method</b>	<b>TractoInferno</b>	<b>HCP</b>	<b>Penthera-3T</b>
sd_stream	1,6M	687,5K	3,6M
ifod2	8,0M	769,7K	3,4M
ptt	8,7M	2,1M	8,7M
TTL	7,7M	1,7M	8,1M
SAC-1k	5,4M	3,9M	14,0M
SAC-3k	<b>11,0M</b>	3,0M	14,0M
CrossQ-3k	4,7M	3,5M	14,0M
SAC-IRT	8,9M	<b>5,7M</b>	<b>22,2M</b>
CrossQ-IRT	10,2M	4,6M	20,7M

like sd\_stream, ifod2 and ptt. The oracle contributes to a more balanced and anatomically accurate streamline generation across evaluation metrics and datasets.

Second, while the ISMRM2015 dataset does not reveal a clear winner among the RL variants, results on the *in vivo* TractoInferno, HCP and Penthera-3T datasets clearly demonstrate the superiority of the IRT scheme. Across the three datasets and all three filtering pipelines, IRT-enhanced methods produce up to  $30\times$  more true positive streamlines than traditional baselines and up to  $1.5\times$  more than their non-IRT RL counterparts.

Additional experimental findings show that extending training to 3,000 episodes (compared to 1,000) does not introduce instability or evidence of reward hacking, further highlighting the robustness of the oracle framework. Furthermore, using shorter streamlines with 32 points—as opposed to 64 or 128—does not compromise the oracle’s accuracy, while substantially reducing computational cost during both training and inference.

The effectiveness of the IRT scheme is further illustrated in Figure 4, which tracks the accuracy of the oracle network during RL training on three datasets using RecobundlesX as a reference. Each data point represents the classification performance on streamlines generated by the RL agent every 50

training episodes. The left-hand plots depict training without IRT, while the right-hand plots show results with IRT. In all cases, the reward network was pre-trained on a dataset different from the one used for the agent’s training, resulting in initially low accuracy due to domain shift. Nevertheless, the IRT mechanism successfully mitigates this domain gap throughout training, steadily improving the reward model’s accuracy.

We observe from our results in table 2 that the overlap of the methods tend to decrease as we extend the agents’ training and as we further increase the number of VC streamlines. We hypothesize that the agents might learn to avoid the edges of the bundles as those edges tend to yield a lower expected cumulative reward in the long run. As there’s some stochasticity in the decision making process of an agent, the agents can easily take a wrong turn leading them to exit the tracking mask (potentially in an undesired region), thus prematurely exiting the tracking procedure which potentially lowers the expected reward in the previously visited states. We suspect that tackling this open question could help to propel RL-based tractography algorithms to having a state of the art coverage while having a best in class generation of plausible streamlines.

Building on the insights of this study, several avenues for future research emerge. We here trained several oracles-one for each filtering algorithm-in order to get a fast-performing and relatively light-weight neural network that reproduces the behaviour of only a single filtering method. As each filtering method currently has their own different biases on the anatomy, we could consider having a neural network that is trained to mimic the behaviour of an aggregation of filtering algorithms. Potentially using those filtering methods in a voting system to attribute target scores to a much larger dataset of streamlines. Naturally, to capture the many complex constraints given by the filtering algorithms, a bigger neural network might be needed. As this work didn’t explore different oracle architectures, we suspect that the avenue of scaling up the capabilities of the oracle could be an interesting topic to address, especially in a scenario with multiple filtering algorithms. As we limited our approach on scaling the number of points used to represent each streamline to a fixed number of 32, one could probably even resample the streamlines to half that number, making room in the prediction time to scale up the size of the model. Such scaling could also potentially directly benefit our methodology as we found it was harder for the oracle to learn the complex constraints posed by `extractor_flow`. Indeed, the oracle is only inputted the geometry (i.e. the directions) of the streamline while the `extractor_flow`



considered more than only the geometry, causing the learning of the oracle to be harder with less information.

As our results suggest a performance plateau for locally informed tracking strategies, future efforts should focus on developing RL policies capable of integrating more global anatomical context. This could involve incorporating long-range dependencies, using hierarchical policies, or leveraging multi-scale representations of the white matter structure. Additionally, extending the current framework to handle uncertainty and ambiguity in more anatomically complex or degenerated regions remains an open challenge. Another crucial direction involves the systematic validation of these models in pathological cases, such as multiple sclerosis or brain tumors, where structural alterations pose significant challenges to existing tractography methods. Finally, improving the interpretability and clinical usability of RL-based tractography systems will be essential for broader adoption in neuroimaging and neurosurgical planning.

## 6. Conclusion

In this work, we extended the TractOracle-RL framework by incorporating recent advances in reinforcement learning, including CrossQ, DroQ, and an iterative training scheme for the reward network. These enhanced variants were systematically evaluated on a range of diffusion MRI datasets, including both *in silico* and *in vivo* data. Our findings reveal that incorporating anatomical priors via reward-based mechanisms consistently improves tractography performance compared to both traditional methods and oracle-free RL baselines. We found this to be also true when extending the training over a larger number of episodes. This highlights the inherent stability and robustness of oracle-guided approaches. The proposed *Iterative Reward Training* (IRT) scheme not only enhances the oracle’s accuracy during training, but also leads to a substantial increase in the number of true positive streamlines generated by the tracking policy, highlighting the importance of incorporating an accurate and robust anatomical signal.

Collectively, these contributions advance the state of RL-based tractography and lay the groundwork for future developments in learning-based white matter reconstruction—particularly in scenarios demanding robust domain adaptation and efficient inference.

## 7. Acknowledgement

This work is in part supported by the Natural Sciences and Engineering Research Council of Canada (RGPIN-2023-04584 and RGPIN-2020-04818) and the institutional USherbrooke Research Chair in Neuroinformatics.

## References

- [1] P. J. Basser, S. Pajevic, C. Pierpaoli, J. Duda, A. Aldroubi, In vivo fiber tractography using dt-mri data, *Magnetic resonance in medicine* 44 (4) (2000) 625–632.
- [2] W. I. Essayed, F. Zhang, P. Unadkat, G. R. Cosgrove, A. J. Golby, L. J. O’Donnell, White matter tractography for neurosurgical planning: A topography-based review of the current state of the art, *NeuroImage: Clinical* 15 (2017) 659–672.
- [3] N. Soni, A. Mehrotra, S. Behari, S. Kumar, N. Gupta, Diffusion-tensor imaging and tractography application in pre-operative planning of intra-axial brain lesions, *Cureus* 9 (10) (2017).
- [4] H. Takemura, J. Kruper, T. Miyata, A. Rokem, Tractometry of human visual white matter pathways in health and disease, *Magn Reson Med Sci.* 23 (3) (2024) 316–340.
- [5] F. Henderson, K. Abdullah, R. Verma, S. Brem, Tractography and the connectome in neurosurgical treatment of gliomas: the premise, the progress, and the potential., *Neurosurg Focus.* 48 (2) (2020).
- [6] F. Zhang, A. Daducci, Y. He, S. Schiavi, C. Seguin, R. E. Smith, C.-H. Yeh, T. Zhao, L. J. O’Donnell, Quantitative mapping of the brain’s structural connectivity using diffusion mri tractography: A review, *NeuroImage* 249 (2022) 118870.
- [7] T. Sarwar, K. Ramamohanarao, A. Zalesky, Mapping connectomes with diffusion mri: deterministic or probabilistic tractography?, *Magn Reson Med* 81 (2) (2019) 1368–1384.
- [8] K. H. Maier-Hein, P. F. Neher, J.-C. Houde, M.-A. Côté, E. Garyfallidis, J. Zhong, M. Chamberland, F.-C. Yeh, Y.-C. Lin, Q. Ji, et al., The challenge of mapping the human connectome based on diffusion tractography, *Nature communications* 8 (1) (2017) 1349.
- [9] B. Jeurissen, A. Leemans, J.-D. Tournier, D. Jones, J. Sijbers, Investigating the prevalence of complex fiber configurations in white matter tissue with diffusion magnetic resonance imaging, *Hum Brain Mapp* 34 (11) (2013) 2747–2766.
- [10] J.-F. Mangin, P. Fillard, Y. Cointepas, D. Le Bihan, V. Frouin, C. Poupon, Toward global tractography, *Neuroimage* 80 (2013) 290–296.

- [11] D. Christiaens, M. Reisert, T. Dhollander, S. Sunaert, P. Suetens, F. Maes, Global tractography of multi-shell diffusion-weighted imaging data using a multi-tissue model, *Neuroimage* 123 (2015) 89–101.
- [12] B. W. Kreher, I. Mader, V. G. Kiselev, Gibbs tracking: a novel approach for the reconstruction of neuronal pathways, *Magnetic Resonance in Medicine: An Official Journal of the International Society for Magnetic Resonance in Medicine* 60 (4) (2008) 953–963.
- [13] R. Smith, J. Tournier, F. Calamante, A. Connelly, Sift: Spherical-deconvolution informed filtering of tractograms., *Neuroimage* 67 (2013) 298–312.
- [14] R. Smith, J. Tournier, F. Calamante, A. Connelly, Sift2: Enabling dense quantitative assessment of brain white matter connectivity using streamlines tractography, *Neuroimage* 119 (2015) 338–351.
- [15] A. Daducci, A. Dal Palu, A. Lemkaddem, J. Thiran, Commit: Convex optimization modeling for microstructure informed tractography., *IEEE Trans Med Imaging* 34 (1) (2015) 246–257.
- [16] K. Petit, L. amd Ali, F. Rheault, A. Bore, S. Cremona, F. Corsini, A. De Benedictis, M. Descoteaux, S. Sarubbo, The structural connectivity of the human angular gyrus as revealed by microdissection and diffusion tractography., *Brain Structure and Function* 228 (1) (2023) 103–120.
- [17] P. Astolfi, R. Verhagen, L. Petit, E. Olivetti, S. Sarubbo, J. Masci, D. Boscaini, P. Avesani, Supervised tractogram filtering using geometric deep learning, *Medical Image Analysis* 90 (2023) 102893.
- [18] J. H. Legarreta, L. Petit, F. Rheault, G. Theaud, C. Lemaire, M. Descoteaux, P.-M. Jodoin, Filtering in tractography using autoencoders (finta), *Medical Image Analysis* 72 (2021) 102126.
- [19] P. F. Neher, M.-A. Côté, J.-C. Houde, M. Descoteaux, K. H. Maier-Hein, Fiber tractography using machine learning, *Neuroimage* 158 (2017) 417–429.
- [20] P. Poulin, M.-A. Côté, J.-C. Houde, L. Petit, Neher, P. F, K. H. Maier-Hein, H. Larochelle, M. Descoteaux, Learn to track: Deep learning for tractography, in: *proc of MICCAI*, Springer, 2017, p. 540–547.
- [21] L. Y. Cai, H. H. Lee, N. R. Newlin, C. I. Kerley, P. Kanakaraj, Q. Yang, G. W. Johnson, D. Moyer, K. G. Schilling, F. Rheault, B. A. Landman, Convolutional-recurrent neural networks approximate diffusion tractography from t1-weighted mri and associated anatomical context, in: *Medical Imaging with Deep Learning*, Vol. 227, 2024, pp. 1124–1143.

- [22] P. Poulin, D. Jorgens, P.-M. Jodoin, M. Descoteaux, Tractography and machine learning: Current state and open challenges, *Magnetic Resonance Imaging* 24 (2019) 37–48.
- [23] J. Wasserthal, P. Neher, K. H. Maier-Hein, Tractseg-fast and accurate white matter tract segmentation, *NeuroImage* 183 (2018) 239–253.
- [24] F. Rheault, A. De Benedictis, A. Daducci, C. Maffei, C. M. W. Tax, D. Romascano, E. Caverzasi, F. C. Morency, F. Corrivetti, F. Pestilli, G. Girard, G. Theaud, I. Zemmoura, J. Hau, K. Glavin, K. M. Jordan, K. Pomiecko, M. Chamberland, M. Barakovic, N. Goyette, P. Poulin, Q. Chenot, S. S. Panesar, S. Sarubbo, L. Petit, M. Descoteaux, Tractostorm: The what, why, and how of tractography dissection reproducibility, *Human Brain Mapping* 41 (7) (2020) 1859–1874.
- [25] M.-A. Côté, G. Girard, A. Boré, E. Garyfallidis, J.-C. Houde, M. Descoteaux, Tractometer: Towards validation of tractography pipelines, *Medical Image Analysis* 17 (7) (2013) 844–857.
- [26] P. Poulin, G. Theaud, F. Rheault, E. St-Onge, A. Bore, E. Renaud, L. de Beaumont, S. Guay, P.-M. Jodoin, M. Descoteaux, Tractoinferno-a large-scale, open-source, multi-site database for machine learning dmri tractography, *Scientific Data* 9 (1) (2022) 725.
- [27] A. Théberge, C. Desrosiers, M. Descoteaux, P.-M. Jodoin, Track-to-learn: A general framework for tractography with deep reinforcement learning, *Medical Image Analysis* 72 (2021) 102093.
- [28] A. Théberge, C. Desrosiers, A. Boré, M. Descoteaux, P.-M. Jodoin, What matters in reinforcement learning for tractography, *Medical Image Analysis* 93 (2024) 103085.
- [29] A. Théberge, M. Descoteaux, P.-M. Jodoin, Tractoracle: towards an anatomically-informed reward function for rl-based tractography, in: *International Conference on Medical Image Computing and Computer-Assisted Intervention*, Springer, 2024, pp. 476–486.
- [30] J. Skalse, N. Howe, D. Krashennnikov, K. D., Defining and characterizing reward hacking, in: *in proc of NeurIPS*, 2022, pp. 9460 – 9471.
- [31] J. Tournier, F. Calamante, D. Gadian, A. Connelly, Direct estimation of the fiber orientation density function from diffusion-weighted mri data using spherical deconvolution, *NeuroImage* 23 (3) (2004) 1176–1185.
- [32] M. Descoteaux, R. Deriche, T. Knösche, A. Anwander, Deterministic and probabilistic tractography based on complex fibre orientation distributions, *IEEE Trans Med Imaging* 28 (2) (2009) 269–286.

- [33] T. Haarnoja, A. Zhou, P. Abbeel, S. Levine, Soft actor-critic: Off-policy maximum entropy deep reinforcement learning with a stochastic actor, in: in proc of ICML, Pmlr, 2018, pp. 1861–1870.
- [34] A. Vaswani, N. Shazeer, N. Parmar, J. Uszkoreit, L. Jones, A. N. Gomez, L. Kaiser, I. Polosukhin, Attention is all you need, *Advances in neural information processing systems* 30 (2017).
- [35] G. Girard, K. Whittingstall, R. Deriche, M. Descoteaux, Towards quantitative connectivity analysis: reducing tractography biases, *Neuroimage* 98 (2014) 266–278.
- [36] E. Renauld, A. Théberge, L. Petit, J.-C. Houde, M. Descoteaux, Validate your white matter tractography algorithms with a reappraised isrmr 2015 tractography challenge scoring system, *Scientific Reports* 13 (1) (2023) 2347.
- [37] E. Garyfallidis, M. Brett, M. M. Correia, G. B. Williams, I. Nimmo-Smith, Quickbundles, a method for tractography simplification, *Frontiers in neuroscience* 6 (2012) 175.
- [38] F. Rheault, Analyse et reconstruction de faisceaux de la matière blanche, Ph.D. thesis, Université de Sherbrooke Computer Science (2020).
- [39] M. Janner, J. Fu, M. Zhang, S. Levine, When to trust your model: Model-based policy optimization, *Advances in neural information processing systems* 32 (2019).
- [40] X. Chen, C. Wang, Z. Zhou, K. Ross, Randomized ensembled double q-learning: Learning fast without a model, *arXiv preprint arXiv:2101.05982* (2021).
- [41] T. Hiraoka, T. Imagawa, T. Hashimoto, T. Onishi, Y. Tsuruoka, Dropout q-functions for doubly efficient reinforcement learning, in: *International Conference on Learning Representations*, 2022.
- [42] A. Bhatt, D. Palenicek, B. Belousov, M. Argus, A. Amiranashvili, T. Brox, J. Peters, Crossq: Batch normalization in deep reinforcement learning for greater sample efficiency and simplicity, in: in proc of ICLR, 2024.
- [43] F. L. Sinzinger, R. Moreno, Reinforcement learning based tractography with so (3) equivariant agents, in: *Geometric Deep Learning in Medical Image Analysis (Extended abstracts)*, 2022.
- [44] P. P. Ray, Chatgpt: A comprehensive review on background, applications, key challenges, bias, ethics, limitations and future scope, *Internet of Things and Cyber-Physical Systems* 3 (2023) 121–154.
- [45] E. Garyfallidis, M.-A. Côté, F. Rheault, J. Sidhu, J. Hau, L. Petit, D. Fortin, S. Cunnane, M. Descoteaux, Recognition of white matter bundles using local and global streamline-based registration and clustering, *NeuroImage* 170 (2018) 283–295.

- [46] K. Maier-Hein, P. Neher, J.-C. Houde, E. Caruyer, A. Daducci, T. Dyrby, B. Stieltjes, M. Descoteaux, Tractography challenge ISMRM 2015 data, 10.5281/zenodo.572345 (2015).
- [47] P. F. Neher, F. B. Laun, B. Stieltjes, K. H. Maier-Hein, Fiberfox: facilitating the creation of realistic white matter software phantoms, *Magnetic resonance in medicine* 72 (5) (2014) 1460–1470.
- [48] J.-D. Tournier, R. Smith, D. Raffelt, R. Tabbara, T. Dhollander, M. Pietsch, D. Christiaens, B. Jeurissen, C.-H. Yeh, A. Connelly, Mrtrix3: A fast, flexible and open software framework for medical image processing and visualisation, *Neuroimage* 202 (2019) 116137.
- [49] E. St-Onge, A. Daducci, G. Girard, M. Descoteaux, Surface-enhanced tractography (set), *NeuroImage* 169 (2018) 524–539.
- [50] B. Mazoyer, E. Mellet, G. Perchey, L. Zago, F. Crivello, G. Jobard, N. Delcroix, M. Vigneau, G. Leroux, L. Petit, et al., Bil&gin: A neuroimaging, cognitive, behavioral, and genetic database for the study of human brain lateralization, *Neuroimage* 124 (2016) 1225–1231.
- [51] S. N. Sotiropoulos, S. Jbabdi, J. Xu, J. L. Andersson, S. Moeller, E. J. Auerbach, et al., Advances in diffusion mri acquisition and processing in the human connectome project, *Neuroimage* 80 (2013) 125–143.
- [52] G. Theaud, J.-C. Houde, A. Boré, F. Rheault, F. Morency, M. Descoteaux, Tractoflow: A robust, efficient and reproducible diffusion mri pipeline leveraging nextflow & singularity, *Neuroimage* 218 (2020) 116889.
- [53] M. Paquette, G. Gilbert, M. Descoteaux, Penthera 3t, <https://doi.org/10.5281/zenodo.2602049>, [Data set] (2019). doi:10.5281/zenodo.2602049.
- [54] D. B. Aydogan, Y. Shi, Parallel transport tractography, *IEEE transactions on medical imaging* 40 (2) (2020) 635–647.
- [55] J. H. Legarreta, L. Petit, F. Rheault, G. Theaud, C. Lemaire, M. Descoteaux, P.-M. Jodoin, Filtering in tractography using autoencoders (finta), *Medical Image Analysis* 72 (2021) 102126.
- [56] D. Silver, G. Lever, N. Heess, T. Degris, D. Wierstra, M. Riedmiller, Deterministic policy gradient algorithms, in: *International conference on machine learning*, Pmlr, 2014, pp. 387–395.
- [57] H. Hasselt, Double q-learning, in: J. Lafferty, C. Williams, J. Shawe-Taylor, R. Zemel, A. Culotta (Eds.), in *proc of NeuRIPS*, Vol. 23, 2010.

- [58] T. Haarnoja, H. Tang, P. Abbeel, S. Levine, Reinforcement learning with deep energy-based policies, in: International conference on machine learning, PMLR, 2017, pp. 1352–1361.
- [59] T. Haarnoja, A. Zhou, K. Hartikainen, G. Tucker, S. Ha, J. Tan, V. Kumar, H. Zhu, A. Gupta, P. Abbeel, et al., Soft actor-critic algorithms and applications, arXiv preprint arXiv:1812.05905 (2018).
- [60] N. Srivastava, G. Hinton, A. Krizhevsky, I. Sutskever, R. Salakhutdinov, Dropout: a simple way to prevent neural networks from overfitting, The journal of machine learning research 15 (1) (2014) 1929–1958.
- [61] J. L. Ba, J. R. Kiros, G. E. Hinton, Layer normalization, arXiv preprint arXiv:1607.06450 (2016).
- [62] S. Ioffe, C. Szegedy, Batch normalization: Accelerating deep network training by reducing internal covariate shift, in: International conference on machine learning, pmlr, 2015, pp. 448–456.
- [63] T. P. Lillicrap, J. J. Hunt, A. Pritzel, N. Heess, T. Erez, Y. Tassa, D. Silver, D. Wierstra, Continuous control with deep reinforcement learning, arXiv preprint arXiv:1509.02971 (2015).
- [64] K. Ota, D. K. Jha, A. Kanezaki, Training larger networks for deep reinforcement learning, arXiv preprint arXiv:2102.07920 (2021).
- [65] K. Ota, T. Oiki, D. Jha, T. Mariyama, D. Nikovski, Can increasing input dimensionality improve deep reinforcement learning?, in: International conference on machine learning, PMLR, 2020, pp. 7424–7433.
- [66] K. He, X. Zhang, S. Ren, J. Sun, Deep residual learning for image recognition, in: Proceedings of the IEEE conference on computer vision and pattern recognition, 2016, pp. 770–778.

## Appendix A. Details of reinforcement learning algorithms

### Appendix A.1. Soft Actor-Critic

---

#### Algorithm 1 Soft Actor-Critic

---

**Require:**  $\theta, \phi_1, \phi_2, \phi'_1, \phi'_2, \alpha, \eta, \bar{\mathcal{H}}$

```

1: for every epoch do
2:   while  $t \neq T$  do
3:      $a_t \sim \pi_\theta(s_t)$ 
4:      $s_{t+1} \sim p(s_{t+1}|s_t, a_t)$ 
5:      $D \leftarrow D \cup (s_t, a_t, r_t, s_{t+1})$ 
6:      $\{(s_k, a_k, r_k, s_{k+1})\} \leftarrow B$  // B: Replay buffer
7:      $\alpha \leftarrow \alpha \eta \nabla_\alpha J_\pi(\alpha)$ 
8:      $\theta \leftarrow \theta \eta \nabla_\theta J_\pi(\theta)$ 
9:      $\phi_1 \leftarrow \eta \nabla \phi_1 J_Q(\phi_1)$ 
10:     $\phi_2 \leftarrow \eta \nabla \phi_2 J_Q(\phi_2)$ 
11:     $\phi'_1 \leftarrow \tau \phi_1 + (1 - \tau) \phi'_1$ 
12:     $\phi'_2 \leftarrow \tau \phi_2 + (1 - \tau) \phi'_2$ 
13:   end while
14: end for
```

---

The Soft Actor-Critic (SAC) algorithm builds upon the Deterministic Policy Gradient theorem [56] which formulates the RL objective as

$$J_\pi(\theta) = \int_S \rho^\pi Q_\phi^{\pi_\theta}(s, a) ds|_{a=\pi_\theta(s)} \quad (\text{A.1})$$

with  $\rho^\pi$  the state-visitation probability density of  $\pi$  and  $Q_\phi^{\pi_\theta}(\mathbf{s}_t, \mathbf{a}_t) = \mathbb{E}_{\pi_\theta}[r_t + G_{t+1} | \mathbf{s}_t, \mathbf{a}_t]$ . Therefore, it follows that the policy update can rely solely on  $Q$ :

$$\nabla_\theta J_\pi(\theta) = \mathbb{E}_{\mathbf{s} \sim \rho^\pi} [\nabla_a Q_\phi^{\pi_\theta}(s, a) \nabla_\theta \pi_\theta(s)|_{a=\pi_\theta(s)}] \quad (\text{A.2})$$

The Q-function, conversely, is trained to minimize the Temporal Difference (TD) via mean-squared error:

$$J_Q(\phi) = \mathbb{E}_{\mathbf{s}_t, \mathbf{a}_t \sim B} \frac{1}{2} [Q_\phi^{\pi_\theta}(s_t, a_t) - \hat{y}]^2 \quad (\text{A.3})$$

$$\hat{y}_t = r_t + \gamma Q_{\phi'}^{\pi_\theta}(s_{t+1}, a_{t+1}) \quad (\text{A.4})$$

$$\nabla_\phi J_Q(\phi) = [Q_\phi^{\pi_\theta}(s_t, a_t) - \hat{y}] \nabla_\phi, \quad (\text{A.5})$$

with  $\phi'$  the weights of a *target* Q-function used to stabilize training and  $\hat{y}$  is the TD target. However, Q-functions tend to suffer from an overestimation bias [57]. SAC therefore uses two Q-functions and two targets  $\phi_1, \phi_2, \phi'_1, \phi'_2$ :



$$\hat{y} = r_t + \gamma \min(Q_{\phi'_1}^{\pi_\theta}(s_{t+1}, a_{t+1}), Q_{\phi'_2}^{\pi_\theta}(s_{t+1}, a_{t+1})) \quad (\text{A.6})$$

$$\nabla_{\phi_1} J_Q(\phi_1) = [Q_{\phi_1}^{\pi_\theta}(s_t, a_t) - \hat{y}] \nabla_{\phi_1} \quad (\text{A.7})$$

$$\nabla_{\phi_2} J_Q(\phi_1) = [Q_{\phi_2}^{\pi_\theta}(s_t, a_t) - \hat{y}] \nabla_{\phi_2}. \quad (\text{A.8})$$

Moreover, to fight the usual sensitivity of RL algorithms to their hyperparameters, the authors exploit the Maximum Entropy Reinforcement Learning framework [58] to augment the previously mentioned RL objective with an entropy maximization term:

$$G_t = \sum_{k=t}^T \gamma^k [r(\mathbf{s}_{t+k}, \mathbf{a}_{t+k}) + \alpha \mathcal{H}(\pi_\theta(\cdot | \mathbf{s}_{t+k}))]. \quad (\text{A.9})$$

Following the updated objective, the Q-function target can be rewritten as:

$$\hat{y} = r_t + \gamma \min(Q_{\phi'_1}^{\pi_\theta}(s_{t+1}, a_{t+1}), Q_{\phi'_2}^{\pi_\theta}(s_{t+1}, a_{t+1})) - \alpha \log \pi_\theta(s_t | a_t). \quad (\text{A.10})$$

$$(\text{A.11})$$

Simiarly, the policy update becomes:

$$\nabla_\theta J_\pi(\theta) = \mathbb{E}_{s \sim \rho^\pi} [\nabla_\theta \log \pi_\theta(a|s) + (\nabla_a \log \pi_\theta(a|s) - \nabla_a Q_{\phi}^{\pi_\theta}(s, a)) \nabla_\theta \pi_\theta(s) |_{a=\pi_\theta(s)}] \quad (\text{A.12})$$

Finally, in a follow-up paper [59], the authors demonstrated that the  $\alpha$  parameter can be automatically tuned using the following objective:

$$J(\alpha) = \mathbb{E}_{a_t \sim \pi_\theta(s_t)} [-\alpha \log \pi_\theta(a_t | s_t) - \alpha \bar{\mathcal{H}}], \quad (\text{A.13})$$

with  $\bar{\mathcal{H}}$  the desired final entropy. All in all, the SAC algorithm can be summarized by Algorithm 1.

## Appendix A.2. DroQ

To improve on sample efficiency, the authors of Dropout Q-functions [41] therefore propose to raise the Update-to-Data (UTD) ratio of SAC above its standard value of 1. The UTD controls the ratio of optimization steps (i.e. lines 5-12 in algorithm 1) to sample gathering steps (lines 3-4). Sample gathering steps may be computationally expensive in complex scenarios and intuitively, performing more optimization steps should lead to a faster convergence. However, it also empirically leads to a higher overestimation bias by the Q-function(s). Some methods [57, 40] have proposed to use more ( $\geq 2$ ) critics to fight this overestimation but this also leads to more memory and computation needed for each optimization step.

Dropout Q-functions [41] has been proposed as a way to increase the UTD without amplifying the overestimation bias while keeping a low (2) number of critics. The authors argue a high number of critics injects model uncertainty into the Q target, which fights overestimation. Instead, the authors include dropout [60] and layer normalization [61] layers in the critics.

### Appendix A.3. CrossQ

While a higher UTD does lead to better sample efficiency, it also leads to more computation as more optimization steps are performed. In an effort to improve sample efficiency while reducing computational costs, CrossQ [42] was proposed. The algorithm removes target Q functions, which require additional computation and instead uses Batch Normalization [62] in the critics’ networks.

While Batch Norm. has been tried for RL before, it was either not included in the critic networks [63, 64] or deemed harmful [42]. The authors of CrossQ argue BatchNorm can be useful as long as the distribution of input states and action is respected. Indeed, target networks  $Q_{\phi'}$  are often updated via polyak averaging of the actual Q networks  $Q_{\phi}$ . However, Q networks are used to compute  $Q_{\phi'}(s_t, a_t)$  from "old" policies (stored as transitions in the replay buffer) while target networks are used to compute  $Q_{\phi'}(s_{t+1}, a_{t+1})$ , with  $a_{t+1} \sim \pi_{\theta}(s_{t+1})$  the current policy. The authors argue the running statistics for  $s_t, a_t$  and  $s_{t+1}, a_{t+1}$  do not match and degrade the quality of predictions from networks with BatchNorm layers.

Instead, the authors propose to match the statistics of  $s_t, a_t$  and  $s_{t+1}, a_{t+1}$  by feeding them jointly to the same network: target Q networks are omitted and  $s_t, s_{t+1}, a_t, a_{t+1}$  are concatenated batch-wise and input to the Q functions. This trick ensures that Batch Norm’s normalizing moments occur from the union of both batches, corresponding to an equal contribution of both batches in calculating the normalization running statistics.

The Q-function objective and update can therefore be re-written as

$$[\hat{q}_t, \hat{q}_{t+1}] = Q_{\phi}^{\pi_{\theta}}([s_t, s_{t+1}], [a_t, a_{t+1}]) \quad (\text{A.14})$$

$$\hat{y} = r_t + \gamma \hat{q}_{t+1} \quad (\text{A.15})$$

$$\nabla_{\phi} J_Q(\phi) = [\hat{q}_t - \hat{y}] \nabla_{\phi}. \quad (\text{A.16})$$

## Appendix B. Oracle architecture

Figure B.7 offers an overview of the oracle’s architecture. The streamlines resampled to a fixed number of points (e.g. 32, 64 or 128 points) are initially transformed into 31 directions by performing a first difference along each neighbouring point. This trips off any position information to only keep the general geometry of the streamline that is used to predict its anatomical plausibility. Each direction (and the CLS token) is then embedded into a vector of size 32 that will then be positionally encoded before being fed to the 4 transformer encoding blocks. From the output of the transformer, we use the CLS token as input to the prediction head (a linear layer of size 32) followed by a sigmoid which produces our prediction value ranging from 0 to 1. For experiments of section 4.6.1, the architecture stays the same, but the input would change to 64 or 128 points.

## Appendix C. fODF neighbourhood autoencoder

The encoder used to encode a wider diffusion signal neighbourhood is a convolutional autoencoder, as shown in figure C.8, which was trained to compress and reconstruct patches of 9x9x9 voxels from the diffusion signal. As it is only used as an experiment

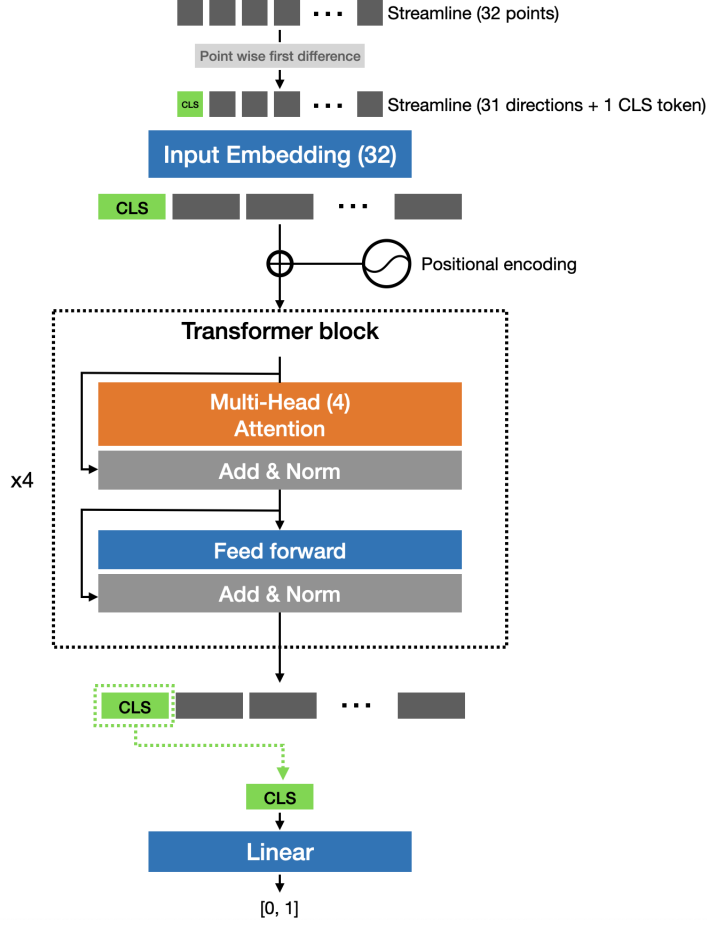


Figure B.7: Architecture of the oracle used in our experiments that is directly inspired by [34]. Inputs in this figure are streamlines represented by 32 (x, y, z) points. For more stable and accurate predictions, the oracle predicts on the directions between each point of the streamline rather than predicting on the (x, y, z) values of the points. This transformer is composed of 4 transformer blocks each having 4 multi-head attention blocks.

for the ISMRM2015 dataset, it was trained on patches randomly selected between all the possible patches that have the central voxel within the white matter region. By learning in a self-supervised way to compress and reconstruct different patches, the encoder eventually learns to extract meaningful representations of the input into a latent space that is approximately 23x smaller than the input. Once the self-supervised training is done, we leverage and meaningful representations learned by the encoder as new inputs for the RL agents so that each state encapsulate a wider context that can be leveraged by the agent.

We chose to decouple the representation learning from the RL training loop as it has been shown that this strategy helped learning in complex scenarios [65, 64]. In addition,

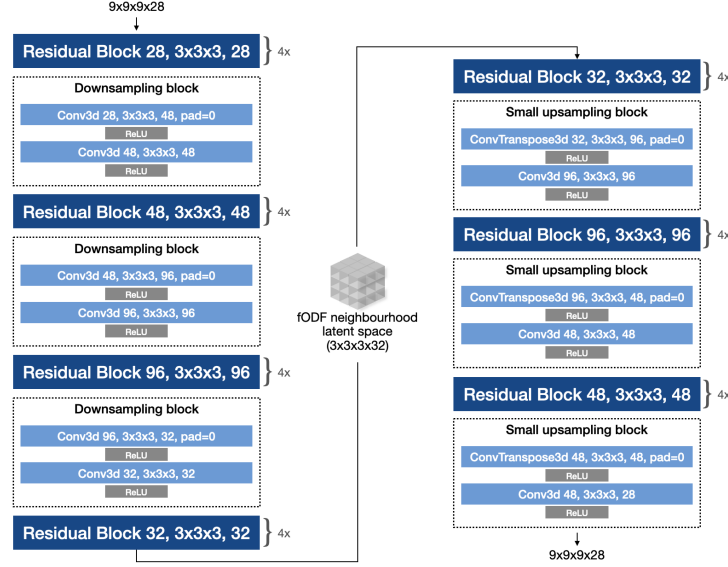


Figure C.8: Architecture of the fODF neighbourhood autoencoder. This network takes a patch of 9x9x9x28 from the ISMRM2015 diffusion signal volume as input, compresses it to a latent representation of shape 3x3x3x32 and learned to faithfully reconstruct the input. Each block holding a convolution is suffixed with "input channels, 3d filter size, output channels". The residual block is inspired from [66] and is simply a Conv3D-BatchNorm-ReLU-Conv3D-BatchNorm block where the number of channels is constant and the input is summed to the output of those layers.

since the encoder parameters are fixed, this allows to reduce considerably the number of parameters to optimize during the training loop which consequentially also limits the time and the computational resources needed to run the RL training loop.

## Appendix D. List of acronyms for ISMRM2015 metrics

- VC: percentage of streamlines exhibiting a valid connection.
- VB: number of valid bundles (max 21).
- IC: percentage of streamlines exhibiting an invalid connection.
- IB: number of invalid bundles connecting regions that should not be connected.
- OL: Overlap (percentage of ground truth voxels recovered).
- OR: Overreach. Quantifies how the algorithm extends past the volume of the ground-truth (percentage of false positive voxels).
- F1: F1-Score, equivalent to the Dice score. The higher the value (max 1), the more the reconstruction volume matches the volume of the ground truth.
- NC: percentage of streamlines that do not connect two gray-matter regions.

## Appendix E. Experiments hyperparameters

Table E.5: **TractOracle-Net training configuration**. Key hyperparameters which were used to initially train the oracles. The same hyperparameters were used to train oracles on the different references (i.e. Tractometer, Recobundles, extractor\_flow or Verifyber). Only the data and the labels change between experiments.

Hyperparameter	Value
Oracle Train Steps (nb epochs)	50
Oracle Learning Rate	0.0005
Oracle Batch Size	1024

Table E.6: **RL training configuration, ISMRM2015**. Key hyperparameters which were used in all RL-based experiments. When performing iterative reward tuning, the extra configuration is used with the rest of the configuration that’s normally used.

Hyperparameter	Value
<i>Experiment parameters</i>	
Number of seed per voxel (NPV)	2
Min. Streamline Length	20
Max. Streamline Length	200
Binary Stopping Threshold	0.1
Angle stopping criterion (degrees)	30
RNG seed	1111
<i>Training configuration (SAC, CrossQ)</i>	
Learning Rate	0.0005
Max Episodes	(1000   3000)
Replay Buffer Size	1,000,000
Number of Directions	100 (4 for TrackToLearn experiments)
Discount Factor ( $\gamma$ )	0.95 (0.75 for TrackToLearn experiments)
Initial entropy coefficient ( $\alpha_{\text{init}}$ )	0.2
Update-to-Data Ratio (UTD)	1 (5 for DroQ)
Hidden Dimensions	1024-1024-1024
Batch Size	4096
Number of Actors	4096
Oracle Bonus	10 (0 for TrackToLearn experiments)
Neighborhood Radius	1 (grid of radius 9 for CrossQ-AE)
<i>Extra configuration for IRT training</i>	
Number of IRT iterations	60
Warmup Agent Steps	150 (SAC)   200 (CrossQ)
Agent Train Steps	50
Oracle Train Steps (1st IRT iter.)	5
Oracle Train Steps (per IRT iter.)	1
Oracle Learning Rate	0.0005
Nb streamlines per iter.	250k
Max. dataset size	4M
IRT tracking NPV	2
Oracle Batch Size	1024
Reference used for oracle training	Tractometer

Table E.7: **RL training configuration, *in-vivo* datasets.** Key hyperparameters which were used in all RL-based experiments. When performing iterative reward tuning, the extra configuration is used with the rest of the configuration that’s normally used.

Hyperparameter	Value
<i>Experiment parameters</i>	
Number of seed per voxel (NPV)	2
Min. Streamline Length	20
Max. Streamline Length	200
Binary Stopping Threshold	0.1
Angle stopping criterion (degrees)	30
RNG seed	1111
<i>Training configuration (SAC, CrossQ)</i>	
Learning Rate	0.0005
Max Episodes	(1000   3000)
Replay Buffer Size	1,000,000
Number of Directions	100 (4 for TrackToLearn experiments)
Discount Factor ( $\gamma$ )	0.95 (0.75 for TrackToLearn experiments)
Initial entropy coefficient ( $\alpha_{\text{init}}$ )	0.2
Update-to-Data Ratio (UTD)	1
Hidden Dimensions	1024-1024-1024
Batch Size	4096
Number of Actors	4096
Oracle Bonus	10 (0 for TrackToLearn experiments)
Neighborhood Radius	1
<i>Extra configuration for IRT training</i>	
Number of IRT iterations	60
Warmup Agent Steps	150 (SAC)   200 (CrossQ)
Agent Train Steps	50
Oracle Train Steps (1st IRT iter.)	5
Oracle Train Steps (per IRT iter.)	1
Oracle Learning Rate	0.0005
Nb streamlines per iter.	250k
Max. dataset size	4M
IRT tracking NPV	2
Oracle Batch Size	1024
Reference used for oracle training	(Recobundles   extractor_flow   Verifyber)